ACS NANO
Cite This: ACS Nano XXXX, XXX, XXX−XXX
www.acsnano.org
ARTICLE

Structure and Dimension Effects on the Performance of Layered Triboelectric Nanogenerators in Contact-Separation Mode

Xing Yin,[†,‡] Di Liu,[†,‡] Linglin Zhou,[†,‡] Xinyuan Li,[†,‡] Chunlei Zhang,[†,‡] Ping Cheng,[†,‡] Hengyu Guo,[†,‡,§] Weixing Song,[†,⊥] Jie Wang,[*,†,‡] and Zhong Lin Wang[*,†,‡,§]

[†]Beijing Institute of Nanoenergy and Nanosystems, Chinese Academy of Sciences, Beijing 100083, P. R. China
[‡]College of Nanoscience and Technology, University of Chinese Academy of Sciences, Beijing 100049, P. R. China
[§]School of Materials Science and Engineering, Georgia Institute of Technology, Atlanta, Georgia 30332, United States
[⊥]School Department of Chemistry, Capital Normal University, Beijing 100048, P. R. China

Supporting Information

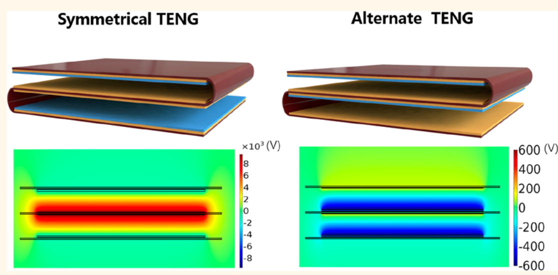

ABSTRACT: **A triboelectric nanogenerator (TENG) is a potential solution for providing high output power by continuously harvesting ambient energy, which is expected to sustainably charge a battery for the new era—the era of the Internet of things and sensor networks. Generally, the existence of parasitic capacitance has been considered to be harmful in its output performance. Here, we systematically investigate the effects of structure and dimension of a TENG on its performance from the point view of parasitic capacitance by fabricating two types of layered TENGs with considering the dissimilarity of the two dielectric materials, symmetrical (ABBA) and alternate (ABAB) layered structure (SYM-TENG and ALT-TENG). Theoretical models of the two types of layered TENGs are proposed for illustrating their differences in parasitic capacitances and output characteristics. Larger parasitic capacitance enables the TENG to accommodate higher triboelectric charge density while reducing the internal impedance and maximum power density. Furthermore, the parasitic capacitance will be enhanced with the decreasing dimension of the devices. The effect of parasitic capacitance on output characteristics of the two kinds of structures are verified in vacuum. Our findings not only establish an optimization methodology for the output performance of TENGs but also provide an insight into the process of triboelectrification.**

KEYWORDS: *triboelectric nanogenerator, structural design, biomechanical energy harvesting, capacitive model, parasitic capacitance*

Harvesting daily wasted energy, such as biomechanical movement, solar irradiation, and wind energy, is an attractive strategy for mitigating expanding energy crises. To satisfy emerging demands for distribution energy sources, various technologies have been demonstrated for harvesting ambient energy, such as triboelectric,[1−5] piezoelectric,[6,7] and pyroelectric.[8,9] Based on triboelectrification and electrostatic induction, triboelectric nanogenerators (TENGs) were developed for converting mechanical energy into electricity in 2012, which has been demonstrated as a promising way to power electronics by scavenging biomechanical, translational, rotatory, and sliding motion energy.[10−12] Based on its basic operating principle, TENG has four fundamental modes, including contact-separation mode,[13] sliding mode,[14] single electrode mode,[15] and a freestanding triboelectric layer mode for diverse practical applications.[16] With its advantage of high output power density, high charge transfer efficiency, and easy integration, contact separation mode shows its great merits working as energy source and active sensor. Many efforts have been devoted to promote output power density of the devices to meet the needs of practical application.[17−23] Generally, a single TENG can deliver approximately microwatt level power which is not enough for high-power consumption electronics. Therefore, fabricating a layered TENG is an effective way to improve output. Much work so far has been focused on the accelerated sensor and energy harvesting of this layered TENG.[20,24] For example, a 10-layer TENG with contacting area of 5.7 cm × 5.2 cm generates about 2.4 μC transferred charge per working cycle. A multiunit TENG of 15 layers (5.7 cm × 5.2 cm) has a maximum instantaneous output power of 19 mW at a frequency of 7 Hz. Indeed, these multiunit TENGs adopted the same structure, where on both sides of the Kapton

Received: October 17, 2018
Accepted: December 19, 2018
Published: December 19, 2018

DOI: 10.1021/acsnano.8b07935
ACS Nano XXXX, XXX, XXX−XXX

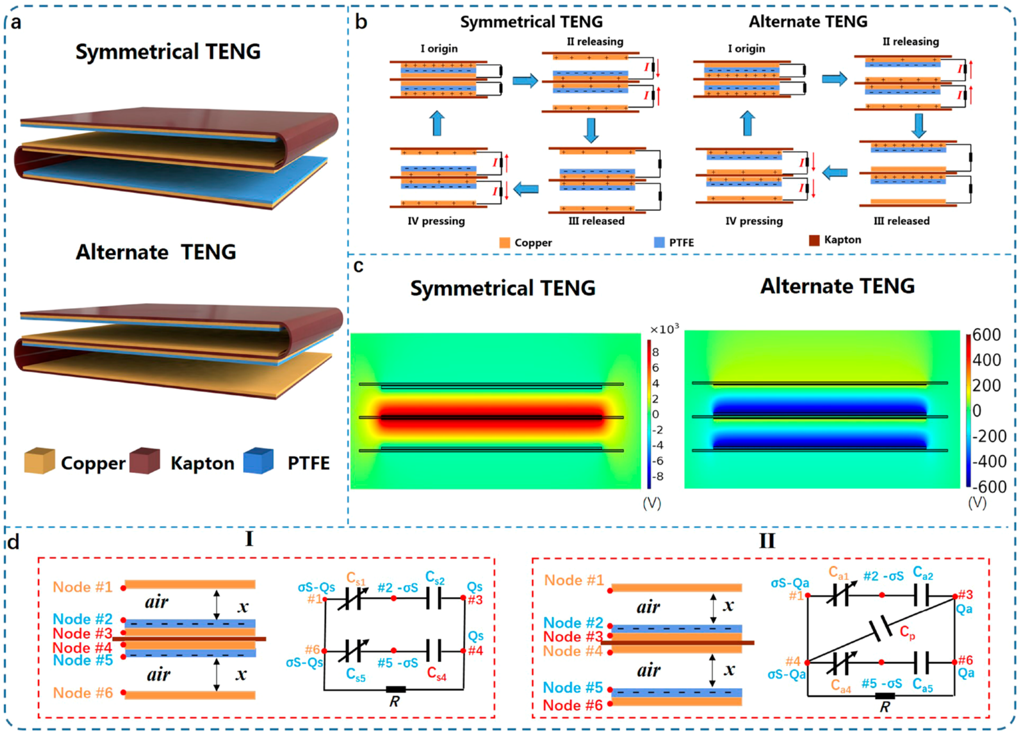

Figure 1. Fabrication and capacitive model analysis of layered TENG. (a) Schematic diagrams of the symmetrical and alternate layered TENG. (b) Working mechanism for SYM-TENG and ALT-TENG. (c) COMSOL simulation for SYM-TENG and ALT-TENG. (d) Model of two units SYM-TENG (I) and ALT-TENG (II) with their corresponding equivalent capacitance circuit.

substrate film, a metal electrode (noted A) and dielectric layer attached metal electrode (noted B) can be constructed into ABAB structure.[25−29] Additionally, ABBA structure in layered TENGs is another choice; it is generally considered that its high parasitic capacitance is harmful in the output performance of TENGs.[30] However, it is not uncovered how parasitic capacitance resulted from structure and dimension design affects the output voltage, current, and charge transfer process of layered TENGs in detail.

In this work, we proposed two capacitive models suitable for symmetrical structure (ABBA) and alternate structure (ABAB) layered TENGs, and considering their structural difference, we illustrate how the parasitic capacitance affects the output performance of a layered TENG theoretically and experimentally. The proposed models show a larger inherent capacitance in alternate layered TENG than that of a symmetrical layered TENG, which are confirmed by experimental results. The output characteristics of two kinds of devices with the same contact area of 5 cm × 5 cm and ten series connected units are systematically investigated. The symmetrical structure reveals a high voltage with less transferred charges, while the alternate structure shows a lower voltage with more transferred charges. This output performance is also verified by vacuum conditions. The two types of structure provide different output characteristics due to the difference of parasitic capacitance, which may be helpful for further understanding the triboelectrification process and structure optimization of TENGs.

RESULTS AND DISCUSSION

The configurations of a layered TENG with two units are schematically illustrated in Figure 1a. There are two ways (ABAB and ABBA) to fabricate a layered TENG noted as ALT-TENG and SYM-TENG, with a metal electrode (noted A) and dielectric layer attached metal electrode (noted B). Here, a Kapton thin film with thickness of 130 μm is introduced as the substrate of the TENG considering its advantageous features of flexibility, light weight, and low cost. It should be noted that, in the symmetrical structure, electrodes on both sides of the Kapton serve as common outputs without parasitic capacitance effects. While for the alternate structure, electrodes on both sides served as two output ends and output voltage is applied on both sides of the Kapton film substrate; therefore, a parasitic capacitor is built with the Kapton film as its dielectric layer. Consequently, SYM-TENG is favorable for avoiding the parasitic capacitance effect. However, ALT-TENG is more desirable for analyzing the parasitic capacitance effect as well as electrostatic induction.

To simplify the working mechanism of layered TENG, the electron transferring mechanism of the two structures is concisely presented in Figure 1b through two units of a layered TENG. (I) With an external force, the SYM-TENG is compressed until the PTFE film and metal electrode contact with each other closely. Because of the different ability in electron affinity, electrons on the metal electrode will transfer to the dielectric layer. (II) After release of the force, electrons on the back electrode can flow through the external load to the metal electrode that is driven by electrostatic induction. As for the symmetrical structure, positive charges accumulate on both sides of the substrate film until the electrostatic equilibrium has been formed. Thus, the net charge on both sides of Kapton films repel each other strongly in symmetrical structure compared to alternate structure, resulting in an equal potential between both electrodes without a parasitic capacitance effect. (III) Once the TENG reaches an electrostatic equilibrium,

DOI: 10.1021/acsnano.8b07935
ACS Nano XXXX, XXX, XXX−XXX

electrons will stop transferring. (IV) When the TENG is compressed again, electrons transfer from the back electrode to the metal electrode until film surfaces fit tightly again (I). After a cycle of external force, alternate current is generated in circuits with different direction for the two structures. Based on the described above, it is found that ALT-TENG actually work in the conventional contact separation mode. Thus, a potential is built between the two electrodes on both sides of Kapton films in alternate structure, which will induce a parasitic effect. For the purpose of distinguishing the two types of layered TENGs theoretically, the electrical potential distribution between metal electrodes was calculated through COMSOL software based on finite element methods. As shown in Figure 1c, when the surface charge density of PTFE films for the two devices was set to be the same value of 50 μC m^{-2} with a gap distance of 3 mm, a much higher open circuit voltage of 8×10^3 V in SYM-TENG can be obtained. The similar results can be found in the two structures with 4, 6, 8, and 10 layers (Supporting Information Figure S1). The potential distribution for the combination of alternate and symmetrical structure TENGs with four units is also simulated. Simulation for the combination of alternate and symmetrical structure TENGs with four units is also shown in Supporting Information Figure S2, which shows the couple of a high potential and a low potential in a layered system. We also investigated the effect of separation distance on open circuit voltage to further discriminating the two types of layered TENGs. As shown in Supporting Information Figure S3, the open circuit voltage increases with increasing separation distance ideally. Note that for SYM-TENG, the open circuit voltage increases with separation distance linearly. However, a different trend is observed for ALT-TENG, wherein the open circuit voltage curve is very similar to a typical capacitor charging curve in shape, indicating the presence of parasitic capacitor in ALT-TENG.

The capacitive models for these two types of layered TENGs are shown in Figure 1d. For the contact-separation mode, total capacitance of a TENG can be equivalent to a variable capacitor in series with an inherent capacitor. Similar to the single TENG capacitive model, the ALT-TENG capacitive model is also composed of variable capacitor and an inherent capacitor. Differently, parasitic capacitance (C_p) is added to the capacitive model of alternate structure that is connected in parallel with external loads and the total capacitance. It is predictable that the total capacitance of device can be enhanced by increasing the layer units of a TENG. In contrast, no parasitic capacitance exists in the SYM-TENG because the same electrical potential distribution in node 3 and 4 that are connected together as a common output. Therefore, output performance of the two structures has been largely determined by the total capacitance. The substrate is Kapton films with a dielectric constant of four. Therefore, parasitic capacitance effect will be weakened when decreasing the dielectric constant.

As reported before,[31] displacement current is the fundamental physical mechanism of TENG, which originated from Maxwell's electromagnetic field theory and the output performance of TENG, including open-circuit voltage, short-circuit current, and triboelectric charge density; this can be simulated through the following analysis based on the proposed capacitive model. A hypothesis should be noted that, if the electrode size is much larger than the gap distance, the electric field edge effect can be neglected. So similar to parallel plate capacitors, we assume the PTFE surface charge density is $-\sigma$ and x is the air gap distance for both structures. Thus, the variable capacitor and inherent capacitor can be derived as follows:

$$C_{s1} = C_{s5} = C_{a1} = C_{a4} = \frac{\varepsilon S}{x} \tag{1}$$

$$C_{s2} = C_{s4} = C_{a2} = C_{a5} = \frac{\varepsilon S}{d} \tag{2}$$

Where S, d, and ε is the area, thickness, and relative permittivity of dielectric material, PTFE, respectively. Therefore, based on the proposed capacitive models, the total capacitance of layered TENGs with two units can be derived:

$$C_s = \frac{2C_{s1}C_{s2}}{C_{s1} + C_{s2}} \tag{3}$$

$$C_a = \frac{2C_{a1}C_{a2}}{C_{a1} + C_{a2}} + C_p = C_s + C_p \tag{4}$$

where C_s and C_a are the total capacitance in symmetrical structure and alternate structure respectively, $C_{s2} = C_{s4} = C_{a2} = C_{a5}$ is the inherent capacitance, and $C_{s1} = C_{s5} = C_{a1} = C_{a4}$ is the air capacitance. As is clear from the above deduction, the total capacitance of ALT-TENG is larger than that of SYM-TENG due to the exit of parasitic capacitance in ALT-TENG.

Generally, inherent capacitor of as-fabricated layered TENG is nearly constant, but parasitic capacitance C_p in alternate structure is in parallel with resistance R that will influence the output performance, and then the corresponding impedance for the two devices can be described as follows

$$Z_s = R \tag{5}$$

$$Z_a = \frac{R}{1 + j\omega RC_p} \tag{6}$$

If a resistance R is connected to the TENG, the equivalent circuit can be described by a capacitor originated and an ideal voltage source (Supporting Information Figure S4). So, the voltage applied on the external load is given by

$$V_s = \frac{RV}{\frac{1}{j\omega RC_s} + R} \tag{7}$$

$$V_a = \frac{C_s}{C_s + C_p}\frac{RV}{\frac{1}{j\omega R(C_s + C_p)} + R} \tag{8}$$

$$\frac{V_a}{V_s} = \frac{C_s}{C_s + C_p}\frac{RV}{\frac{1}{j\omega R(C_s + C_p)} + R}\frac{\frac{1}{j\omega RC_s} + R}{RV} \tag{9}$$

$$\frac{|V_a|}{|V_s|} = = \sqrt{\frac{(\omega RC_s)^2 + 1}{[(\omega R(C_s + C_p)]^2 + 1}} \tag{10}$$

The above equations could help in understanding open circuit voltage for the two devices. It should be noted that the transfer charge $Q = 0$ for both layered TENGs when comparing eqs 7 and 8 under the open circuit condition. Therefore, open circuit voltage in symmetrical structure $|V_s|$ will be larger than that in alternate structure $|V_a|$, which further identifies the result described in Figure 1c. Furthermore, the

DOI: 10.1021/acsnano.8b07935
ACS Nano XXXX, XXX, XXX−XXX

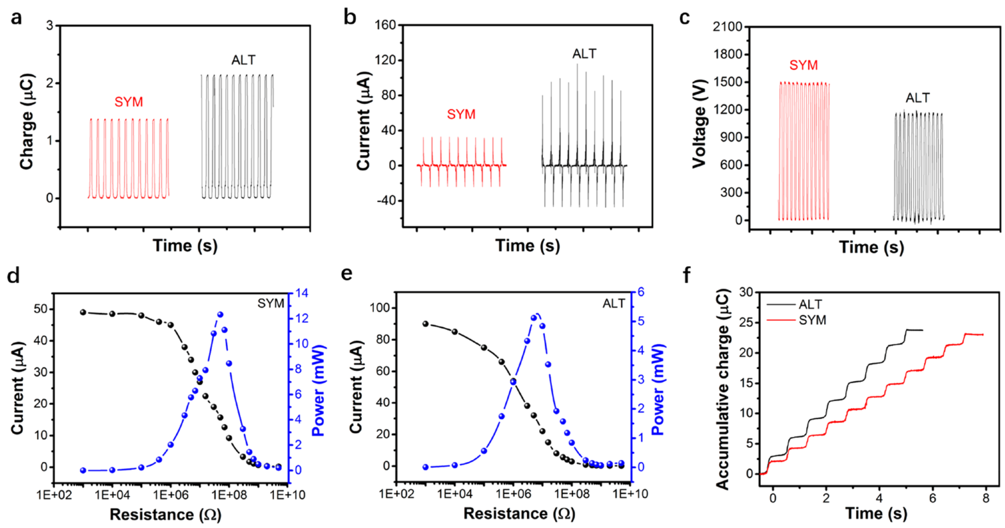

Figure 2. Electrical output performance of the two types of layered TENGs. (a) Transferred charge, (b) short-circuit current, and (c) open-circuit voltage comparison of two layered TENGs. Output current and power of SYM-TENG (d) and ALT-TENG (e) with various external loads. (f) Accumulative charge generated by two structured TENG.

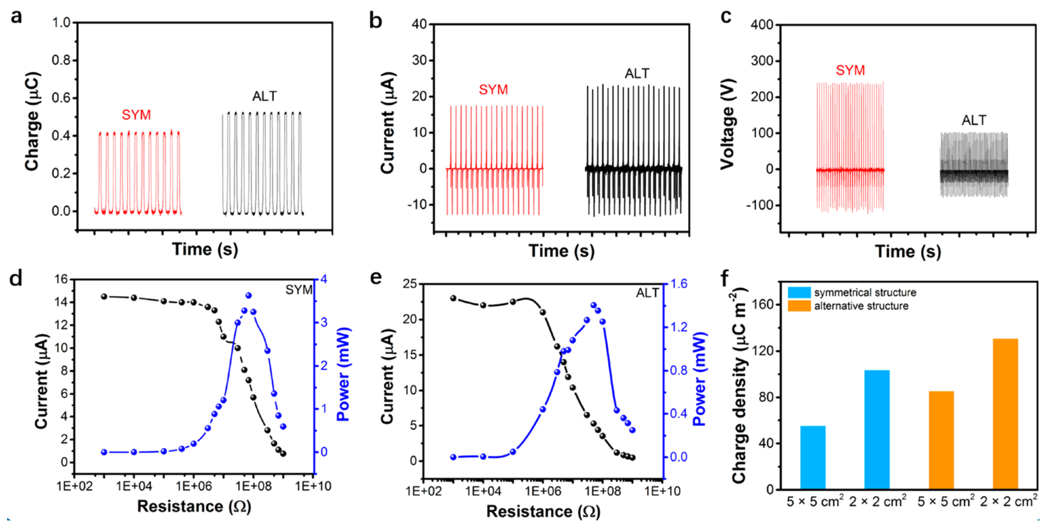

Figure 3. Output performance of small size layered TENG. (a) Amount of transferred charge, (b) short-circuit current, and (c) open-circuit voltage of two layered TENGs. (d, e) Short-circuit current and power density of SYM-TENG (d) and ALT-TENG (e) with various loads. (f) Comparison of electrode size effects on the transferred charge density for the two types of layered TENGs.

average power delivered to the load can be given based on Kirchhoff's law.

$$P_s = \frac{V^2}{R}\left(\frac{R}{\frac{1}{j\omega C_s} + R}\right)^2 \tag{11}$$

$$P_a = \frac{V^2}{R}\left(\frac{C_s}{C_s + C_p}\right)^2 \frac{1}{\left(\frac{1}{\omega R(C_s + C_p)}\right)^2 + 1} \tag{12}$$

$$\frac{|P_a|}{|P_s|} = \frac{(\omega R C_s)^2 + 1}{[\omega R(C_s + C_p)]^2 + 1} \tag{13}$$

The match load of TENG refers to the external load that equals the value of internal resistance, when the output power reached the maximum value. The matched impedance can be derived from the derivative of eqs 7 and 8, as shown in eq 14.

$$R_a = \frac{1}{\omega(C_s + C_p)} R_s = \frac{1}{\omega C_s} \tag{14}$$

According to the capacitive model discussed above, $C_a > C_s$, which is caused by the parasitic capacitance effect. This could theoretically show higher open circuit voltage, high output power, and a higher inner impedance in symmetrical structure than that in alternate structure, which will be also verified by the next part of experimental results.

In order to evaluate the electrical output performance and confirm the proposed capacitive model of two types of layered TENGs, the two kinds of devices are tested and the results are shown in Figure 2. For alternate structure, the transferred charge is 2.15 μC (Figure 2a), which is higher than that of the symmetrical structure (1.37 μC), indicating that ALT-TENG could transfer more charges than SYM-TENG. Correspond-

DOI: 10.1021/acsnano.8b07935
ACS Nano XXXX, XXX, XXX−XXX

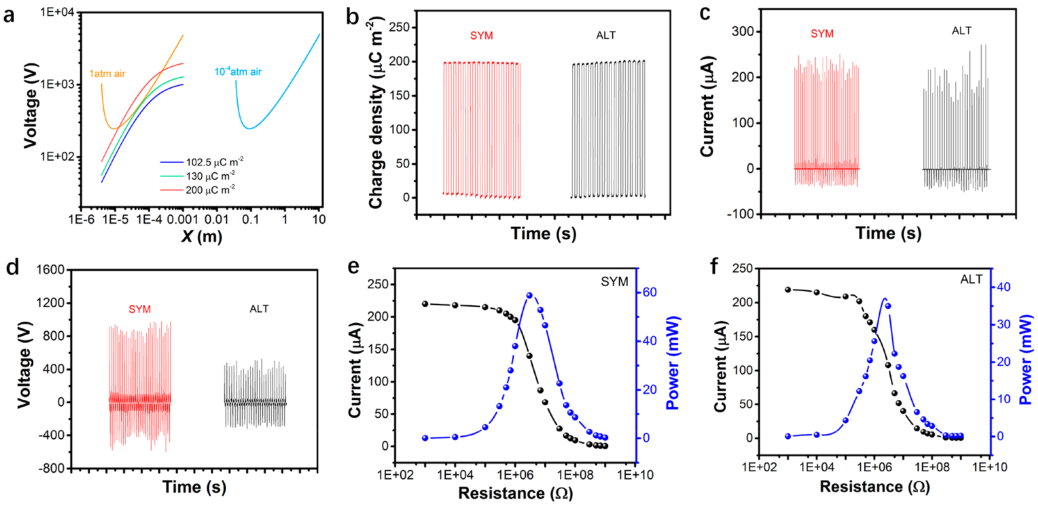

Figure 4. Output performance of two types of layered TENGs in vacuum. (a) Air breakdown voltage and gap voltage with different charge densities. (b) Transferred charge, (c) short-circuit current, (d) open-circuit voltage of SYM-TENG and ALT-TENG in vacuum conditions. Output power of SYM-TENG (e) and ALT-TENG (f).

ingly, the peak value of short-circuit current increases from 33.48 μA in ALT-TENG to 107.24 μA in SYM-TENG (Figure 2b). However, the symmetrical structure with less transferred charge could deliver a higher open circuit voltage 1500 V than that of 1180 V in alternate structure (Figure 2c), further confirming the above theoretical analysis. Interestingly, the maximum output power of SYM-TENG reaches up to 12.3 mW, about 2.4-fold that of the ALT-TENG (5.12 mW) as shown in Figure 2d and e, i.e. ALT-TENG with more charges delivers lower peak power due to the parasitic capacitance effect. Through the full wave rectifier bridge, alternating signals can be changed to direct signals. Due to the difference of the total transferred charge in the two types of layered TENG, the accumulative charge of ALT-TENG reaches 25 μC in 6 s, which is 2 s faster than that of the SYM-TENG, in good accordance with its higher transferred charge quantity in ALT-TENG (Figure 2f). Therefore, the existence of parasitic capacitance is beneficial for enhancing the transferred charge and decreasing matched resistance but harmful to the peak power density.

It is known that the contact area can greatly influence output performance of TENGs. Besides, the effective contact area plays an important role in the process of charge transfer, whereas the amount of transferred charge is not proportional to the area of triboelectric layer.[32] Herein, ALT-TENG and SYM-TENG with smaller size (2 cm × 2 cm) are fabricated to further investigate the two types of layered TENG. As displayed in Figure 3a, the amount of transferred charge increases from 0.41 μC in symmetrical structure to 0.52 μC in alternate structure. Accordingly, the short-circuit current rises from 17.33 to 27.85 μA (Figure 3b), the open circuit voltage decreases from 358 to 177 V (Figure 3c), and the maximum output power density is reduced from 3.6 mW at a load of 70 MΩ to 1.4 mW at a load of 50 MΩ (Figure 3d, e). Importantly, layered TENGs with smaller dimensions (2 cm × 2 cm) exhibit a higher ability to accommodate larger charge density, wherein their charge density is nearly 2 times higher than that of the TENG with the size of 5 cm × 5 cm (Figure 3f) due to the enhanced contact effectivity.

Ideally, the electric field in a parallel plate capacitor has a uniform distribution in space, and the field lines also stay parallel. Whereas, the closer to the edge of the plates, the more field lines will be bent; this phenomenon of electric field divergence is commonly called the edge effect. Generally, the edge effect can effectively enhance the air capacitance when reducing metal electrode area (Supporting Information Figure S5).[15] Therefore, when decreasing the size of a layered TENG, the influence of the edge effect on parasitic capacitance for ALT-TENG can be enhanced.[27] As shown in Supporting Information Figure S6, since decreasing the size from 5 cm × 5 cm to 2 cm × 2 cm, the tested capacitance of the ALT-TENG becomes larger than theoretical capacitance. Because of the lager parasitic capacitance with smaller size inducing by the edge effect, a TENG with size of 2 cm × 2 cm produces a lower open circuit voltage (Supporting Information Figure S7), thus contributing to a higher transferred charge density as displayed in Figure 3f. For the 2 cm × 2 cm TENG, the comparison V_{sym}/V_{alt} is 2.02, which is higher than that, 1.27, in the 5 cm × 5 cm TENG. Meanwhile, the comparison of transferred charge Q_{sym}/Q_{alt} with the size of 2 cm × 2 cm is 0.79, which is also higher than that, 0.31, in the 5 cm × 5 cm TENG. It is furthermore verified by the comparison P_{SYM}/P_{ALT} = 2.40 with an area of 5 cm × 5 cm and P_{SYM}/P_{ALT} = 2.57 with an area of 2 cm × 2 cm.

It is extremely obscure to understand the physical mechanisms of contact electrification process, which are largely determined by many environmental factors, such as air breakdown, temperature, humidity, and contaminants on dielectric or electrode surfaces. Furthermore, the phenomenon of air breakdown is verified by ion injection method.[21] As can be seen in Supporting Information Figure S8, the surface charge density of the PTFE film with a thickness of 200 μm reaches its maximum value of 135 μC m^{-2} in the atmosphere, which is the theoretical limitation of air breakdown. Based on the relationship between air breakdown voltage and gap voltage with different charge density as shown in Figure 4a, the performance enhancement of TENGs can be significantly improved by using high vacuum. Hence, the vacuum environment is an effective way to investigate the proposed capacitance of two devices. Without air breakdown, the transfer charge is improved to 200 μC m^{-2} for both layered TENGs with contact areas of 2 cm × 2 cm in a vacuum

DOI: 10.1021/acsnano.8b07935
ACS Nano XXXX, XXX, XXX−XXX

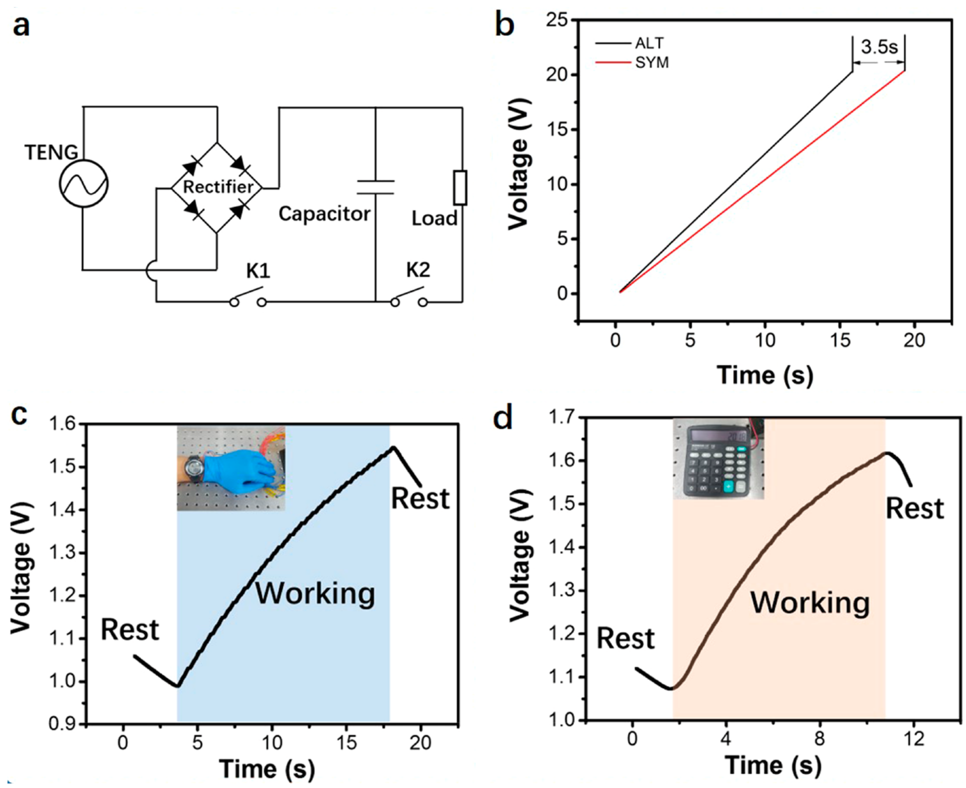

Figure 5. Application of the two types of layered TENGs for powering electronic devices. (a) Circuit diagram of the self-powered system consisting of a layered TENG and a capacitor. (b) Charging curves of a capacitor (2.2 μF) powered by two structure of TENGs. (c) Electronic watch and (d) calculator powered by the ALT-TENG.

environment with a pressure of 10^{-4} Pa (Figure 4b). Besides the same transfer charge, the short circuit current of both structures remains almost the same since it is determined by dQ/dt (Figure 4c). However, the open circuit voltage in the symmetrical structure is about 1.8-fold that in the alternate structure (Figure 4d), and the peak power density of SYM-TENG is nearly 1.7 times that of ATL-TENG (Figure 4e, f). These results demonstrate that parasitic capacitance also takes effect in vacuum conditions without the influence of other environmental factors, which also decrease the open circuit voltage and the power density of the layered TENG.

The ability of outputting high voltage and a high amount of transferred charges through the alternate and symmetrical structure leaves the layered TENG with more choices when dealing with different application areas. The output performance of two devices with a contact area of 5 cm × 5 cm for practical application was shown in Figure 5 through powering electronic devices. Figure 5a is the circuit diagram of the self-powered system integrating a TENG and a capacitor by a full wave rectifier. Note that when the TENG is applied to charge a capacitor directly, the most important output characteristic is high transfer charge density rather than high output voltage. Operating by the linear motor at a frequency of 1 Hz, it takes 15.8 s for the ALT-TENG to charge the capacitor from 0 to 20 V, while it takes 19.3 s for SYM-TENG to do the same as shown in Figure 5b, which shows the fast charging ability of ALT-TENG (Supporting Information Figure S9). Furthermore, Figure 5c presents an electrical watch powered by manually pressing the ALT-TENG (Supporting Information Video S1). When the layered TENG was mounted under a pair of shoes, an electronic watch can be sustainably lit up by walking (Supporting Information Video S2). A calculator powered by ALT-TENG is also shown in Figure 5d (Supporting Information Video S3). Moreover, the TENG with high output voltage may have great potential for application in air purification, electrostatic adsorption, et al.

CONCLUSIONS

In summary, we fabricated two types of layered TENGs with alternate and symmetrical structures. The two devices display diverse output in that a higher transfer charge density in ALT-TENG and a higher open circuit voltage in SYM-TENG are achieved, respectively, due to the existence of parasitic capacitance in the ALT-TENG. With the higher output voltage, the output power density of the SYM-TENG can be 2.4 times higher than that of the ALT-TENG. The small size layered TENG demonstrates the enhancement of parasitic capacitance by edge effects when decreasing the dimensions of the TENG. Then power reduction will be more obvious. The effect of parasitic capacitance on output characteristics of the two kinds of layered TENGs are verified in vacuum conditions. The effectiveness of the layered TENG for sustainably powering the wearable electronics by harvesting biomechanical energy is successfully demonstrated. Finally, our results not only illustrate an effective strategy to achieve high voltage or high charge density when scaling up layered TENG in commercial application but also provide an insight into the triboelectrification process that results in an extra parasitic capacitance.

METHODS

Fabrication of Layered Triboelectric Nanogenerators. As for the ALT-TENG, a Kapton film with thickness of 130 μm was folded into a zigzag with 10 layers, acting as the substrate. Then a Cu film

DOI: 10.1021/acsnano.8b07935
ACS Nano XXXX, XXX, XXX−XXX

with an area of 5 cm × 5 cm is adhered to the both sides of the Kapton film. Then PTFE layers were attached on both sides of the Cu layer every other layer in a symmetrical structure or attached on the same side of the Cu layer in alternate structure. The small dimension TENGs with size of 2 cm × 2 cm used for studying size effects were fabricated by the same method.

Comsol Simulation. The potential distribution of two structured devices was calculated by the commercial software COMSOL. The width of the TENG was set to be 1 cm, and the thickness of the Cu electrode and PTFE films were 60 and 200 μm, respectively. The gap distance of Cu and PTFE was 3 mm, and the surface charge density was 50 μC m^{-2}.

Characterization. The short-circuit current and transferred charges were measured by a programmable electrometer (Keithley model 6514). The open-circuit voltage was obtained by an oscilloscope (MODI 3014). The contact-separation process and its output performance were obtained by a vacuum system.

ASSOCIATED CONTENT

Supporting Information

The Supporting Information is available free of charge on the ACS Publications website at DOI: 10.1021/acsnano.8b07935.

Figures S1−S9 providing the COMSOL simulation of the layered TENG and the combination of alternate and symmetrical structure TENGs; open circuit voltage-separation distance relationship of the layered TENG; simplified equivalent circuit of the layered TENG; influence of electrode length on C/C_0; parasitic capacitance and open-circuit voltage of layered TENG; theoretical calculation of maximum surface charge density; the charging curves of a commercial capacitor (PDF)

Video S1: electronic watch powered by manually pressing the ALT-TENG (AVI)

Video S2: electronic watch sustainably lit up by walking (AVI)

Video S3: calculator powered by a linear motor (AVI)

AUTHOR INFORMATION

Corresponding Authors

*Email: wangjie@binn.cas.cn (J.W.).

*Email: zhong.wang@mse.gatech.edu (Z.L.W.).

ORCID

Jie Wang: 0000-0003-4470-6171

Zhong Lin Wang: 0000-0002-5530-0380

Author Contributions

X.Y. and D.L. contributed equally to this work.

Notes

The authors declare no competing financial interest.

ACKNOWLEDGMENTS

This research was supported by the National Key R & D Project from Minister of Science and Technology (2016YFA0202704), Beijing Municipal Science & Technology Commission (Z171100000317001, Z171100002017017, Y3993113DF), and National Natural Science Foundation of China (Grant No. 61774016, 21773009, 51432005, 5151101243, 51561145021).

REFERENCES

(1) Fan, F.-R.; Tian, Z.-Q.; Wang, Z. L. Flexible Triboelectric Generator! *Nano Energy* **2012**, *1*, 328−334.

(2) Wang, J.; Li, X. H.; Zi, Y. L.; Wang, S. H.; Li, Z. L.; Zheng, L.; Yi, F.; Li, S. M.; Wang, Z. L. A Flexible Fiber-Based Supercapacitor-Triboelectric-Nanogenerator Power System for Wearable Electronics. *Adv. Mater.* **2015**, *27*, 4830−4836.

(3) Wang, J.; Wen, Z.; Zi, Y. L.; Zhou, P. F.; Lin, J.; Guo, H. Y.; Xu, Y. L.; Wang, Z. L. All-Plastic-Materials Based Self-Charging Power System Composed of Triboelectric Nanogenerators and Super-capacitors. *Adv. Funct. Mater.* **2016**, *26*, 1070−1076.

(4) Wang, Z. L. Triboelectric Nanogenerators As New Energy Technology and Self-Powered Sensors - Principles, Problems and Perspectives. *Faraday Discuss.* **2014**, *176*, 447−458.

(5) Wang, J.; Wen, Z.; Zi, Y.; Lin, L.; Wu, C.; Guo, H.; Xi, Y.; Xu, Y.; Wang, Z. L. Self-Powered Electrochemical Synthesis of Polypyrrole from the Pulsed Output of a Triboelectric Nanogenerator As a Sustainable Energy System. *Adv. Funct. Mater.* **2016**, *26*, 3542−3548.

(6) Zheng, Q.; Shi, B.; Li, Z.; Wang, Z. L. Recent Progress on Piezoelectric and Triboelectric Energy Harvesters in Biomedical Systems. *Adv. Sci.* **2017**, *4*, 1700029.

(7) Liu, W.; Zhang, A.; Zhang, Y.; Wang, Z. L. Density Functional Studies on Wurtzite Piezotronic Transistors: Influence of Different Semiconductors and Metals on Piezoelectric Charge Distribution and Schottky Barrier. *Nanotechnology* **2016**, *27*, 205204.

(8) Wang, X.; Dai, Y.; Liu, R.; He, X.; Li, S.; Wang, Z. L. Light-Triggered Pyroelectric Nanogenerator Based on a pn-Junction for Self-Powered Near-Infrared Photosensing. *ACS Nano* **2017**, *11*, 8339−8345.

(9) Wang, S.; Wang, Z. L.; Yang, Y. A One-Structure-Based Hybridized Nanogenerator for Scavenging Mechanical and Thermal Energies by Triboelectric-Piezoelectric-Pyroelectric Effects. *Adv. Mater.* **2016**, *28*, 2881−2887.

(10) Zhu, G.; Chen, J.; Zhang, T.; Jing, Q.; Wang, Z. L. Radial-Arrayed Rotary Electrification for High Performance Triboelectric Generator. *Nat. Commun.* **2014**, *5*, 3426.

(11) Shang, W.; Gu, G. Q.; Yang, F.; Zhao, L.; Cheng, G.; Du, Z. L.; Wang, Z. L. A Sliding-Mode Triboelectric Nanogenerator with Chemical Group Grated Structure by Shadow Mask Reactive Ion Etching. *ACS Nano* **2017**, *11*, 8796−8803.

(12) Yi, F.; Wang, J.; Wang, X.; Niu, S.; Li, S.; Liao, Q.; Xu, Y.; You, Z.; Zhang, Y.; Wang, Z. L. Stretchable and Waterproof Self-Charging Power System for Harvesting Energy from Diverse Deformation and Powering Wearable Electronics. *ACS Nano* **2016**, *10*, 6519−6525.

(13) Niu, S.; Wang, S.; Lin, L.; Liu, Y.; Zhou, Y. S.; Hu, Y.; Wang, Z. L. Theoretical Study of Contact-Mode Triboelectric Nanogenerators As an Effective Power Source. *Energy Environ. Sci.* **2013**, *6*, 3576−3583.

(14) Niu, S.; Liu, Y.; Wang, S.; Lin, L.; Zhou, Y. S.; Hu, Y.; Wang, Z. L. Theory of Sliding-Mode Triboelectric Nanogenerators. *Adv. Mater.* **2013**, *25*, 6184−6193.

(15) Niu, S.; Liu, Y.; Wang, S.; Lin, L.; Zhou, Y. S.; Hu, Y.; Wang, Z. L. Theoretical Investigation and Structural Optimization of Single-Electrode Triboelectric Nanogenerators. *Adv. Funct. Mater.* **2014**, *24*, 3332−3340.

(16) Niu, S.; Liu, Y.; Chen, X.; Wang, S.; Zhou, Y. S.; Lin, L.; Xie, Y.; Wang, Z. L. Theory of Freestanding Triboelectric-Layer-Based Nanogenerators. *Nano Energy* **2015**, *12*, 760−774.

(17) Chun, J.; Ye, B. U.; Lee, J. W.; Choi, D.; Kang, C. Y.; Kim, S. W.; Wang, Z. L.; Baik, J. M. Boosted Output Performance of Triboelectric Nanogenerator *via* Electric Double Layer Effect. *Nat. Commun.* **2016**, *7*, 12985.

(18) Cheng, G.; Lin, Z.-H.; Du, Z.; Wang, Z. L. Increase Output Energy and Operation Frequency of a Triboelectric Nanogenerator by Two Grounded Electrodes Approach. *Adv. Funct. Mater.* **2014**, *24*, 2892−2898.

(19) Wang, Q.; Chen, M.; Li, W.; Li, Z.; Chen, Y.; Zhai, Y. Size Effect on the Output of a Miniaturized Triboelectric Nanogenerator Based on Superimposed Electrode Layers. *Nano Energy* **2017**, *41*, 128−138.

(20) Zi, Y.; Wu, C.; Ding, W.; Wang, Z. L. Maximized Effective Energy Output of Contact-Separation-Triggered Triboelectric Nano-

generators As Limited by Air Breakdown. *Adv. Funct. Mater.* **2017**, *27*, 1700049.
(21) Wang, S.; Xie, Y.; Niu, S.; Lin, L.; Liu, C.; Zhou, Y. S.; Wang, Z. L. Maximum Surface Charge Density for Triboelectric Nanogenerators Achieved by Ionized-Air Injection: Methodology and Theoretical Understanding. *Adv. Mater.* **2014**, *26*, 6720−6728.
(22) Wang, J.; Wu, C.; Dai, Y.; Zhao, Z.; Wang, A.; Zhang, T.; Wang, Z. L. Achieving Ultrahigh Triboelectric Charge Density for Efficient Energy Harvesting. *Nat. Commun.* **2017**, *8*, 88.
(23) Li, S. M.; Wang, J.; Peng, W. B.; Lin, L.; Zi, Y. L.; Wang, S. H.; Zhang, G.; Wang, Z. L. Sustainable Energy Source for Wearable Electronics Based on Multilayer Elastomeric Triboelectric Nanogenerators. *Adv. Energy Mater.* **2017**, *7*, 1602832.
(24) Wang, X.; Niu, S.; Yi, F.; Yin, Y.; Hao, C.; Dai, K.; Zhang, Y.; You, Z.; Wang, Z. L. Harvesting Ambient Vibration Energy over a Wide Frequency Range for Self-Powered Electronics. *ACS Nano* **2017**, *11*, 1728−1735.
(25) Wang, Z. L. On Maxwell's Displacement Current for Energy and Sensors: The Origin of Nanogenerators. *Mater. Mater. Today* **2017**, *20*, 74−82.
(26) Dai, K.; Wang, X.; Niu, S.; Yi, F.; Yin, Y.; Chen, L.; Zhang, Y.; You, Z. Simulation and Structure Optimization of Triboelectric Nanogenerators Considering the Effects of Parasitic Capacitance. *Nano Res.* **2017**, *10*, 157−171.
(27) Peng, J.; Kang, S. D.; Snyder, G. J. Optimization Principles and the Figure of Merit for Triboelectric Generators. *Sci. Adv.* **2017**, *3*, eaap8576.
(28) Niu, S.; Wang, Z. L. Theoretical Systems of Triboelectric Nanogenerators. *Nano Energy* **2015**, *14*, 161−192.
(29) Liu, R. Y.; Wang, J.; Sun, T.; Wang, M. J.; Wu, C. S.; Zou, H. Y.; Song, T.; Zhang, X. H.; Lee, S. T.; Wang, Z. L.; Sun, B. Silicon Nanowire/Polymer Hybrid Solar Cell-Supercapacitor: A Self-Charging Power Unit with a Total Efficiency of 10.5%. *Nano Lett.* **2017**, *17*, 4240−4247.
(30) Niu, S.; Wang, X.; Yi, F.; Zhou, Y. S.; Wang, Z. L. A Universal Self-Charging System Driven by Random Biomechanical Energy for Sustainable Operation of Mobile Electronics. *Nat. Commun.* **2015**, *6*, 8975.
(31) Wang, Z. L.; Jiang, T.; Xu, L. Toward the Blue Energy Dream by Triboelectric Nanogenerator Networks. *Nano Energy* **2017**, *39*, 9−23.
(32) Wang, J.; Li, S.; Yi, F.; Zi, Y.; Lin, J.; Wang, X.; Xu, Y.; Wang, Z. L. Sustainably Powering Wearable Electronics Solely by Biomechanical Energy. *Nat. Commun.* **2016**, *7*, 12744.

DOI: 10.1021/acsnano.8b07935
ACS Nano XXXX, XXX, XXX−XXX